Insights into multiphase reactions during self-discharge of Li-S batteries

Guobin Wen,[a,=] Sarish Rehman,[a,b,=] Tom G. Tranter,[a,c,=] Debasis Ghosh,[d] Zhongwei Chen,[a] Jeff T. Gostick,[a,*] Michael A. Pope[a,b,*]

[a] Department of Chemical Engineering, University of Waterloo, Waterloo, Ontario N2L 3G1, Canada.

[b] Quantum Nano Centre, Department of Chemical Engineering, University of Waterloo, Waterloo, Ontario N2L 3G1, Canada.

[c] Electrochemical Innovation Lab, Department of Chemical Engineering, University College London, Torrington Place, London WC1E 7JE, United Kingdom.

[d] Centre for Nano & Material sciences, JAIN University, Jain Global Campus, Bangalore 562112, India.

[=] These authors contributed equally to this work.

ABSTRACT: Lithium-sulfur (Li-S) batteries are promising next-generation rechargeable energy storage systems due to their high energy density and use of abundant and inexpensive materials. However, rapid self-discharge and poor cycle stability due to the solubility of intermediate polysulfide conversion products have slowed their commercialization. Herein, we provide a detailed account of the multiphasic reactions occurring during self-discharge of a Li-S battery held at various degrees of discharge (DOD) through both simulation and experiment. For the first time, self-discharge of a full Li-S battery is simulated using a 1D model to describe reactions at both the anode and cathode. The model accurately describes experimentally derived results obtained over the longest durations of self-discharge studied to date (140 h). This validated model was used to follow the reversible and irreversible capacity loss caused by shuttling and precipitation of insoluble Li_2S_2 and Li_2S as a function of DOD. While the most rapid self-discharge is observed at low DOD, this also leads to the smallest irreversible loss. The results suggest that resting a Li-S battery near 2.1 V minimizes both reversible and irreversible losses.

1. INTRODUCTION

The lithium-sulfur (Li-S) battery is one of the most promising battery systems owing to its high theoretical specific capacity of 1672 mAh/g and specific energy of 2600 Wh/(kg active material only).[1–3] Unlike intercalation compounds, the transformation of sulfur to Li_2S takes place *via* the formation of a series of intermediate lithium polysulphides (PSs) i.e., Li_2S_n (where, n = 2 – 8).[4,5] The long chain PSs are soluble in the ether-based electrolytes typically used. Consequently, they migrate across the cell and participate in parasitic reactions at the anode or elsewhere in the cell leading to reversible or irreversible capacity loss *via* chemical conversion or precipitation of shorter chain PSs.[6,7] This problem, caused by the mobility of sulfur-containing species, is generally referred to as the PSs shuttling phenomena. Depending on conditions, this shuttling can either passivate or corrode the lithium anode and contributes to self-discharge and low Coulombic efficiency.[2,8,9] To mitigate this, different strategies have been investigated such as the use of additives[10,11] or coatings to protect the lithium surface,[12,13] metal oxide adsorbents[14–19] to capture the PSs, modified separators[20] and cathode designs which aim to stabilize and retain PSs.[21–23] Although the cycle-life improvement associated with these aforementioned strategies is well documented,[13] the time-scale associated with cycling is on the order of a few hours (cycling is typically carried out at 0.5 or 1C for practical reasons), and few studies focus on self-discharge which can occur over days or months when a battery is stored between uses.[24] To accelerate the commercial development of Li-S batteries, it is necessary to gain a deeper understanding of shuttling phenomena and its impact on self-discharge rates over long periods and different resting conditions, so that such capacity losses can be minimized.

Self-discharge is a major obstacle for the development of Li-S batteries. Mikhaylik and Akridge have studied the experimental self-discharge rates for Li-S batteries by quantitatively analysing the shuttle phenomenon.[25] They reported that the primary cause of self-discharge is the migration of soluble PSs (Li_2S_n, $8 < n < 3$) at the higher voltage plateau (~2.33 V vs. Li). Knap et al. investigated the dependence of the self-discharge behavior on the depth of discharge (DOD), resting time, and operational temperature.[26] These works have demonstrated that Li—S batteries suffer a ca-

pacity fade of over 50% in a month or less. In contrast, commercial Li-ion batteries exhibit extremely low self-discharge (less than 3% per month).[27–29] While self-discharge is generally thought to be a result of shuttling, the mechanisms which control the rates and reversibility of the capacity loss are not well understood. While cycling a real battery takes weeks to months, a numerical model can be run in a fraction of the time to provide useful understanding of the key chemical processes and performance, thus there is a strong incentive to develop rigorous models of Li-S batteries.

Recent studies have identified the presence of multifaceted physicochemical interactions during capacity fading, such as precipitation/dissolution dynamics, interfacial kinetics, concentrated solution effects, and poromechanical progression to name a few.[4,30–33] Hofmann et al. presented a mechanistic model to provide insights into the key mechanisms with a focus on shuttling phenomena. However, their model did not take into account the nucleation and growth of solid precipitates.[34] The mathematical models by Busche et al.[35] and Marinescu et al.[36] studied the correlation between the state of discharge and the cell kinetics using a shuttle constant, k_s, which was determine by time-consuming experiments. However, they could not accurately estimate the self-discharge resulting from PSs reduction at the anode. A more complete model was considered by Kumaresan et al.[37] who developed a one-dimensional model of a Li-S cell involving five electrochemical conversion steps in the cathode as well as precipitation/dissolution reactions that form insoluble PSs. However, they were only able to simulate one charge and one discharge. Unfortunately, the complexity of the Li-S system requires not only the assumption of many parameters, but also consideration of the cycling and resting behaviours. After reviewing a range of analytical studies and physical models, it is clear that state-of-the-art models lag behind experimental understanding.[38] The knowledge about mechanisms at the core of Li–S battery models is incomplete compared to the latest thinking based upon experimental results. More effort is needed to verify these results and update the models. Thus, there is a significant need to develop an improved model and to validate against the latest experimentally derived data.

Here, we present the first numerical 1D model of the Li-S battery that take into account the speciation of PSs from the cathode to the anode over long cycling periods, including idling over various depths of discharge. The model provides a deeper insight into the reversible and irreversible capacity loss experienced during self-discharge. Importantly, for the first time, simulation data is compared to extensive experimental data obtained from long cycling and resting periods and the results provide close agreement.

2. EXPERIMENTAL METHOD AND MODEL DESCRIPTION

2.1. Synthesis of acid modified graphene. A commercial graphene nanoplatelet powder (GNPs) was obtained from NanoXplore Inc. (grade DMP-4). Prior to use, this material was modified *via* an acid treatment to increase the level of exfoliation and to provide some oxygen-containing functional groups which are known to interact with polysulfides and somewhat reduce the shuttling phenomena. [39] In a typical synthesis procedure, 1 g of GNP powder and 10 mM sodium dodecyl sulfate (SDS micropellets, molecular biology grade, Fisher bioreagents) was mixed with 500 ml of 18 $M\Omega$ deionized (DI) water then sonicated for 1 hr at 50% power. After sonication, the dispersion was vacuum filtered and washed with 500 mL of DI water. To prevent aggregation of the GNPs, the filter cake was not allowed to dry, and this filter cake was added to 130.4 mL of concentrated sulfuric acid (Sigma Aldrich, 95-98 %) and 113.23 mL nitric acid (Sigma Aldrich, 70 %) (3:2 ratio (vol/vol) which was heated at 50°C for 24h under stirring. The resulting mixture was separated from the residual acids by centrifugation. The supernatant was discarded, and the pellet was washed by filtration with 500-700 mL of DI water. The sample was dried and collected for electrode fabrication.

2.2. Synthesis of graphene nanoplatelets/sulfur composite. The modified GNP/sulfur composite was prepared by mixing 40:60 (mass/mass) of GNP to sulfur using a mortar and pestle for 15 min. The mixture was transferred to an Ar-filled glovebox (< 1ppm air and water) and placed within an autoclave that was sealed within the Ar-filled environment. The autoclave was heated to 160°C for 12h which was sufficient to melt the sulfur and draw liquid into the pores of the graphene-based material via capillary action as molten sulfur is known to wet carbonaceous materials.[40]

2.3. Fabrication of Electrode and Electrochemical Measurement. Sulfur cathodes were prepared by mixing 80 wt.% of active materials (GNP/S), 10 wt.% carbon black powder (carbon super P, MTI) and 10 wt.% of polyvinylidene fluoride (PVDF, Sigma Aldrich, MW ~ 534,000) dissolved in N-methyl-2- pyrrolidone (NMP, Sigma Aldrich 99.5%)) thoroughly to make a slurry. The slurry was then cast onto one side of carbon paper (AvCarb P50 - 40 × 40 cm) and dried in a vacuum oven at 50°C for 12 h for the evaporation of NMP. The sulfur loading was 3.2-5.5 mg cm^{-2} and electrolyte volume was 90 µl (electrolyte to sulfur ratio of ~16:1).

GNP/S cathodes were tested using CR2032-type stainless steel coin cells assembled in an Ar-filled glove box. The cathode was separated from a lithium metal anode (Sigma-Aldrich, thickness 0.75mm, width 45mm, 99.9% trace metal basis) using a polypropylene membrane (25 µm, Celgard 2325). Prior to crimping, 90 µL of an ether-based electrolyte (1:1 (vol/vol) 1,3 - dioxolane (DOL) and 1,2-dimethoxyethane ((DME), containing 0.2 m lithium nitrate ($LiNO_3$) and 1 M lithium bis(trifluoromethane)sulfonimide (LiTFSI) (all from Sigma-Aldrich 99.9%) were added to cell. Galvanostatic cycling was carried out between limits of 1.7 and 2.7 V (vs. Li/Li^+) on a Neware Battery Tester (0V to + 5V, 0.1 A). Based on the mass of elemental sulfur, the gravimetric current density of 1672 mA/g was used to define the C-rate.

The test protocol comprised of five steps and cells were charged and discharged between 2.7-1.7 V. Step 1 corresponds to a pre-condition cycle of charge and discharge. Step 2 involved charging the cell to 2.7 V by a current of 0.1C and discharging to a pre-determined depth of discharge (DOD′, the prime indicates it is the experimental DOD as opposed to the one defined by modelling below) by the same current. The cell was held at open circuit conditions (OCV)

for 48 hr during step 3 and then in step 4 it was fully discharged to 1.7 V. We chose five representative potentials to investigate the behaviour at rest because it took several months to finish one experiment. The DOD′ chosen for self-discharge measurements were specified by the potentials of 2.04 V (~81%, 8th discharge), 2.1 V ~30%,14th discharge), 2.7 V (~ 0%, 21st discharge), 2.25 V (~22 %, 27th discharge) and 1.95 V (~94 %, 33th discharge). Where indicated, the order was changed to confirm there is no cycle number dependence on the self-discharge behavior.

To investigate the precipitation of Li_2S_2(s) and Li_2S(s) within the cell, ex-situ X-ray diffraction (XRD, Rigaku Miniflex II, CuK_α radiation) on the components of a cell (cathode, anode and separator) was carried out. Cells were disassembled after the 11th cycle when the cell was held for self-discharging at ~22% DOD (2.1V) for 48hr and then completely discharged to 1.7 V. The XRD samples were prepared inside the glove box, covered with Kapton film to slow the diffusion of air/moisture which would react with Li_2S and Li_2S_2 to form products such as H_2S.

2.4. Model Description. Figure 1a shows the geometry considered in the study. An attempt was made to include a rigorous treatment of precipitation and polysulfide shuttling. A 1D model was used since it is more practical as computational complexity increases, as does the number of assumed parameters. To match the experimental conditions, the thickness of the separator was set to 25 μm, denoted as L_s, while the thickness of cathode was 36 μm, denoted as L_c. To reduce the model complexity, the anode was considered a point. This assumption was acceptable because lithium was in excess (a thick Li foil is used).

As depicted in Figure 1b, five electrochemical reactions were considered to take place at the cathode (C1 - C5), while one occurred at the anode surface (A1) during charge and discharge per single electron transfer step. Although there was evidence to suggest that charge was not the exact reversal of discharge, the assumption can be made in this case for numerical simplicity.[36,41–44] Figure 1c shows the precipitation/dissolution reactions forming solid PSs that were considered to take place. Depending on the local concentrations of ionic species, one or more of the following precipitates may be formed: Li_2S_8, Li_2S_6, Li_2S_4, Li_2S_2, Li_2S. But previous experimental and simulation studies indicate that all lithium sulfides except Li_2S_2 and Li_2S are substantially soluble in the electrolyte.[37,45–48] In addition to precipitation of Li_2S_2 and Li_2S, the model also includes the precipitation of Li_2S_8 and Li_2S_4 for illustration purposes.

The governing equations of the mathematical model are outlined below. A list of the stoichiometric coefficients of species in reactions is given in Table S1 of the Supporting Information. The current density is given by the Butler-Volmer equation:[37]

$$I_j = I_{0,\mathrm{ref},j}\left[\left(\frac{c_{\mathrm{Re},j}}{c_{\mathrm{Re,ref},j}}\right)^{s_{\mathrm{Re},j}} exp\left(\frac{\alpha_{\mathrm{an}}F\eta_j}{RT}\right) - \left(\frac{c_{\mathrm{Ox},j}}{c_{\mathrm{Ox,ref},j}}\right)^{-s_{\mathrm{Ox},j}} exp\left(\frac{-\alpha_{\mathrm{ca}}F\eta_j}{RT}\right)\right], \quad (1)$$

where I_j is the current density of reaction j, $I_{0,j,\mathrm{ref}}$ is the reference exchange current density, as shown in the Table 1, c_{Re} and c_{Ox} are the concentration of reduced (Re) and oxidized (Ox) species (Ox + ne^- → Re), respectively. c_{ref} is the reference concentration which are also the initial concentration of species in the electrolyte when beginning discharge for the first time, s is the stoichiometric coefficient of reduced or oxidized species. α are the anodic (an) and cathodic (ca) transfer coefficients (both set equal to 0.5), η_j is the overpotential given by:

$$\eta_j = \varphi_{\mathrm{l}} - \varphi_{\mathrm{s}} - U_{j,\mathrm{ref}}, \quad (22)$$

where φ_{l} and φ_{s} are the liquid and solid phase potentials. The liquid phase current density is related to the flux of ionic species, while the solid phase potential is governed by Ohm's Law. $U_{j,\mathrm{ref}}$ is the open circuit potential given by:

$$U_{j,\mathrm{ref}} = U_j^0 - \frac{RT}{n_jF}\left[s_{Re,j} ln\, c_{\mathrm{Re,ref}} - s_{\mathrm{Ox},j} ln\, c_{\mathrm{Ox,ref}}\right] \quad (33)$$

where U_j^0 is the formal potential[49] of reaction j, which is a fitting parameter that encompasses both the standard potential and the activity coefficients of the species; n_j is the number of electrons transferred in the reaction j. Equation (3) is valid only when the concentrations are expressed in moles per liter.[37] The sensitivity analyses of $I_{0,j,\mathrm{ref}}$, U_j^0 , and reference concentrations were performed to validate the values (Figure S1-S3).

Table 1. The kinetic parameters for each reaction

Reactions	$I_{0,j,\mathrm{ref}}$ [A/m²]	U_j^0 [V]
A1	1	0.0
C1	1.972	2.39
C2	0.019	2.37
C3	0.019	2.24
C4	1.97×10^{-4}	2.04
C5	1.97×10^{-7}	2.01

For a multicomponent electrolyte in a porous electrode the conservation of each charged species i (i =Li^+, $S_{8(l)}$, S_8^{2-}, S_6^{2-}, S_4^{2-}, S_2^{2-}, S^{2-}, and A^-, here, A^- denotes the anion of the lithium salt used in the electrolyte) is given by the Nernst-Planck equation:

$$\frac{\partial \varepsilon c_i}{\partial t} = -\nabla N_i + r_i - R_i, \quad (44)$$

where c_i is the concentration, ε represents the pore volume fraction of the porous cathode or separator, N_i is the flux due to diffusion and migration in the potential field, r_i is the electrochemical reaction rate and R_i is the precipitation/dissolution rate. Flux is given by:

$$N_i = -D_i\nabla c_i - z_i\frac{D_i}{RT}Fc_i\nabla\varphi_{\mathrm{l}}, \quad (5)$$

where D_i is the effective diffusion coefficient of species i with the bulk electrolyte species which can be related to the porosity of the material using the Bruggeman relation. (Table S2 and Equation S1 of the Supporting Information)

The electrochemical reaction rate for reaction j is given by:

$$r_i = -S_a\sum_{j=\mathrm{C1}}^{\mathrm{C5}}\frac{s_{i,j}I_j}{n_jF}, \quad (6)$$

where S_a is the electrochemically active surface area per unit volume, $s_{i,j}$ is the stoichiometric coefficient of species i in the reaction j. The surface area is assumed to vary with porosity, which changes over time as elemental sulfur dissolves and PSs precipitate, according to the following relation:

$$S_a = S_{a,0}\left(\frac{\varepsilon}{\varepsilon_0}\right)^{\chi}. \quad (7)$$

where χ is the empirical parameter describing the morphology of the precipitate and is assigned a value of 1.5 in this work.

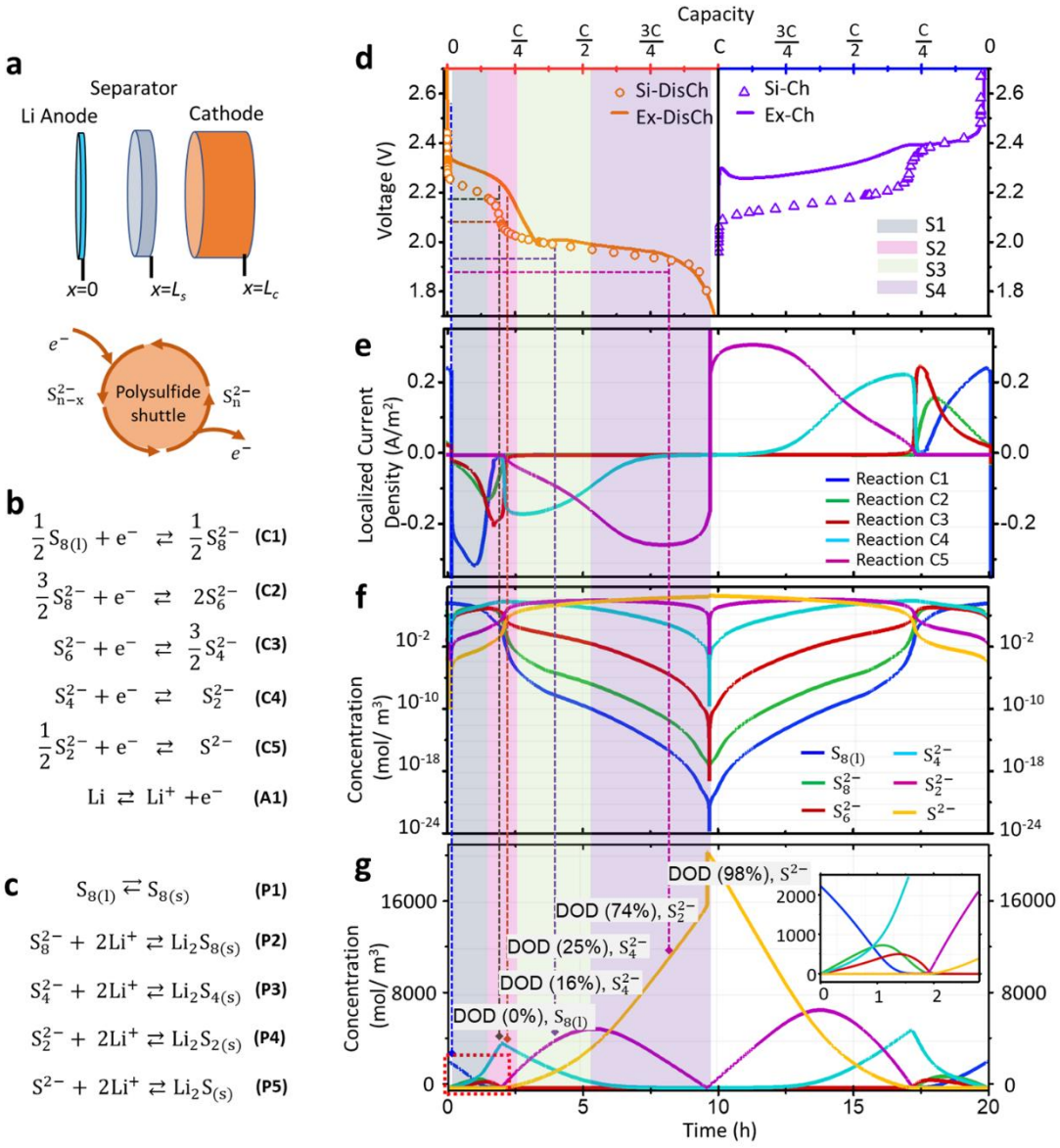

Figure 1. (a) A schematic illustration of the Li-S battery model setup and PS shuttle effect. (b) Electrochemical reactions in the sulfur cathode and lithium anode. (c) Phase change reactions considered in the model. (d) Comparison of experimental (Ex) vs. simulated (Si) voltage profiles during one discharge-charge cycle of Li-S batteries. Simulated localized current density profiles of multi-reactions in cathode (e) and simulated concentration variations of PS during one discharge-charge cycle: (f) y-axes are in in a logarithmic scale; (g) y-axes are in linear scale. Five representative DOD levels were chosen. The discharge profile was divided into four sections in (d-f): S1-dominated by Reaction C1; S2-dominated by Reaction C2 and C3; S3-dominated by Reaction C4; S4-dominated by Reaction C5. The dashed lines correspond to the indicated DOD.

The third term in Equation (44), R_i, describes the rate of precipitation of species i to form solid salts and is important to the present study which considers cycles and periods of rest, and is given as:

$$R_i = \sum_{k=\mathrm{P1}}^{\mathrm{P5}} \gamma_{i,k} R'_k \quad (8)$$

$$= \sum_{k=\mathrm{P1}}^{\mathrm{P5}} \gamma_{i,k} \upsilon_k \varepsilon_k \left(\prod_i c_i^{\gamma_{i,k}} - K_{sp,k} \right)_k ,$$

where R'_k is the rate of precipitation reaction containing solid species k (P1- P5 as shown in Figure 1c), $\gamma_{i,k}$ is the number of moles of species i in the precipitation reactions, υ_k is the rate constant, ε_k is the solid volume fraction of the precipitation k. The precipitation rate (R'_k) is assumed to depend on the solubility product and concentration of related species. The precipitation parameters are shown in Table S3. A sensitivity analysis of the precipitation rate (Figure S4) revealed that the volume fraction of Li_2S_2 increased rapidly and lead to unphysical behavior when increasing the precipitation reaction rate.

The change in total porosity of the electrode is impacted by precipitation/dissolution rate and the molar volume of the precipitating and dissolving species, $\tilde{V}_k$:

$$\frac{\partial \varepsilon}{\partial t} = -\sum_{k=\mathrm{P1}}^{\mathrm{P5}} \frac{\partial \varepsilon_k}{\partial t} = -\sum_{k=\mathrm{P1}}^{\mathrm{P5}} \tilde{V}_k R'_k . \qquad (9)$$

The polysulfide shuttle is essentially composed of two distinct events: shuttling of sulfur species in the electrolyte, and their subsequent chemical reduction at the anode. The species shuttling in the electrolyte has two transport mechanism: diffusion and migration. Concentration gradients lead to diffusion while potential gradients drive migration of PSs. Thus, the species shuttling in the electrolyte is strongly related to the species concentration. These PSs species accept electrons from the Li metal at the anode and are reduced, but the electron is not exchanged in the external circuit. In order to quantify the reactivity of PSs at the anode, Mistry et al.[50] proposed to use a chemical overpotential (η_{ch}) as a fitting parameter, which is analogous to the definition of an electrochemical overpoential. Although the reduction at the anode is different from the electrochemical reduction of sulfur at the cathode, the chemical reactivity (reaction rate, υ_{an}) of the anode characterized by a chemical overpotential (η_{ch}) might be an acceptable strategy:

$$\upsilon_{an,j} = \frac{i_{0,j,\mathrm{ref}}}{F} exp\left(\frac{-F\eta_{\mathrm{ch}}}{2RT}\right) \cdot \left(\frac{c_{\mathrm{Ox},j}}{c_{\mathrm{Ox,ref},j}}\right)^{s_{\mathrm{Ox},j}} , \qquad (10)$$

where $i_{0,j,\mathrm{ref}}$ is the reference exchange current density, which is the same as the definition at the cathode, and η_{ch} is the chemical overpotential. As η_{ch} approaches zero, the anode surface reactions are thermodynamically favored and in turn faster. When larger than 0.5 V, the PSs reduction reactions at the anode become slow, which differs from experimental observations. A sensitivity analysis of η_{ch} on the model output revealed that 0.45 V is a reasonable value that led to the best fit to our experimental data as discussed further in the main text below (Figure S5).

The other parameter values used in the model are listed in Table S4 and the equations of charge conservation are shown in Equation S2-S5. The set of differential and algebraic equations were solved using a finite element solver (COMSOL Multiphysics). A mesh sensitivity study was performed to determine the necessary amount of mesh refinement. Dynamic discharge-charge cycling periods and resting periods were simulated by the *event interface module*. The model predicted the evolution of the species concentrations, together with changes in the porosity of the separator and cathode, and the volume fraction of the different precipitates, across an electrode pair (anode–separator–cathode).

2.5. Definition of Capacity Loss. To provide a clear understanding of capacity lost (CL), a proper understanding of reversible and irreversible capacity fade during resting periods is needed. In terms of experimental data, the CL can only be estimated via coulomb counting. On the other hand, simulations provide the species distribution over each simulation step and enable us to directly quantify the state of each species in the battery. Thus, two different kinds of definitions are provided based on experimental and simulation results, respectively. The following sections discuss each of these.

Intuitive Definition of CL. From an experimental point of view, the CL of the cell or self-discharge behaviour are quantified as follows, where the various capacities are obtained from coulomb counting:[51]

$$C_{\mathrm{t,CL}} = (C_{\mathrm{ini}}, - C_{\mathrm{dod}}, - C_{\mathrm{rem}})/C_{\mathrm{ini}}, , \qquad (11)$$

$$C_{\mathrm{rev,CL}} = (C_{\mathrm{rch}} - C_{\mathrm{dod}}, - C_{\mathrm{rem}})/C_{\mathrm{ini}}, , \qquad (12)$$

$$C_{\mathrm{ir,CL}} = (C_{\mathrm{ini,Ex}} - C_{\mathrm{rch}})/C_{\mathrm{ini}}, , \qquad (13)$$

$$C_{\mathrm{t,CL}} = C_{\mathrm{rev,CL}} + C_{\mathrm{ir,CL}} , \qquad (14)$$

where C_{ini}, is the initial capacity determined during the pre-conditioning cycle (again the primes indicate experimentally derived value); C_{dod}, is the discharge capacity to the specific DOD′ level; C_{rem} is the remaining discharge capacity after resting the cell at a specified voltage; C_{rch} is the capacity exhibited by the cell during recharge after the resting condition; $C_{\mathrm{t,CL}}$ represents the total CL during the resting condition; the reversible CL is $C_{\mathrm{rev,CL}}$, and $C_{\mathrm{ir,CL}}$ is the irreversible CL.

Intrinsic Definition of CL. The model can provide a detailed description of the species which have been lost in the cycle and also the inefficiency of cycling capacity due to self-discharge. Through counting the amount of precipitate directly and, from that, calculating a reduction in total working capacity and the amount of self-discharge current, the relevant losses can be calculated as following:

$$C_{\mathrm{precip,CL}} = \left[2F \cdot \left(c_{\mathrm{Li_2S}} + 2c_{\mathrm{Li_2S_2}} \right)\right]/C_{\mathrm{ini}} , \qquad (15)$$

$$C_{\mathrm{flux,CL}} = \left[FA_C\left(16v_{\mathrm{S_8}} + 14v_{\mathrm{S_8^{2-}}} + 10v_{\mathrm{S_6^{2-}}} + 6v_{\mathrm{S_4^{2-}}} + 2v_{\mathrm{S_2^{2-}}} + v_{\mathrm{S^{2-}}} \right)\right]/C_{\mathrm{ini}} , \qquad (16)$$

where $C_{\mathrm{precip,CL}}$ is the precipitation CL due to the formation of Li_2S and Li_2S_2, which precipitate in the electrolyte and at the anode side; $c_{\mathrm{Li_2S}}$ and $c_{\mathrm{Li_2S_2}}$ are the total number of moles of Li_2S and Li_2S_2, respectively; C_{ini} is the theoretical initial capacity based on species concentration; $C_{\mathrm{flux,CL}}$is the total self-discharge CL due to the shuttle flux and reduction of S_8(l), S_8^{2-}, S_6^{2-}, S_4^{2-} and S_2^{2-} species towards the anode; $v_{\mathrm{S_8}}$, $v_{\mathrm{S_8^{2-}}}$, $v_{\mathrm{S_6^{2-}}}$, $v_{\mathrm{S_4^{2-}}}$, and $v_{\mathrm{S_2^{2-}}}$ represent the self-discharge flux rate of each species, and the unit is mol/(m^2 s).

3. RESULTS AND DISCUSSION

3.1. Model validation, current density and concentration distribution. Figure 1d compares the cell voltages during both discharging and charging measured exper-

imentally with the simulation results. The model qualitatively reproduces essential features of a typical Li–S cell discharge-charge profile. However, there are some noticeable mismatches between the simulated and experiment profiles in the finer details. The mismatch of the voltage profiles might be due to lack of a detailed treatment in the model of nucleation and growth of solid particles. Besides this, the model still reproduces essential features of a Li-S cell well, such as two discharging plateaus and the long experimental cycling capacity losses and satisfy the latest experimentally derived mechanisms. Therefore, the proposed Li-S model provides a significant advance compared to state-of-the-art models but requires furthermore detail be added in future work to capture all mechanistic aspects. However, this will also require more unknown parameters. Future experimental work is needed to help to validate some of the many kinetic and thermodynamic parameters required.

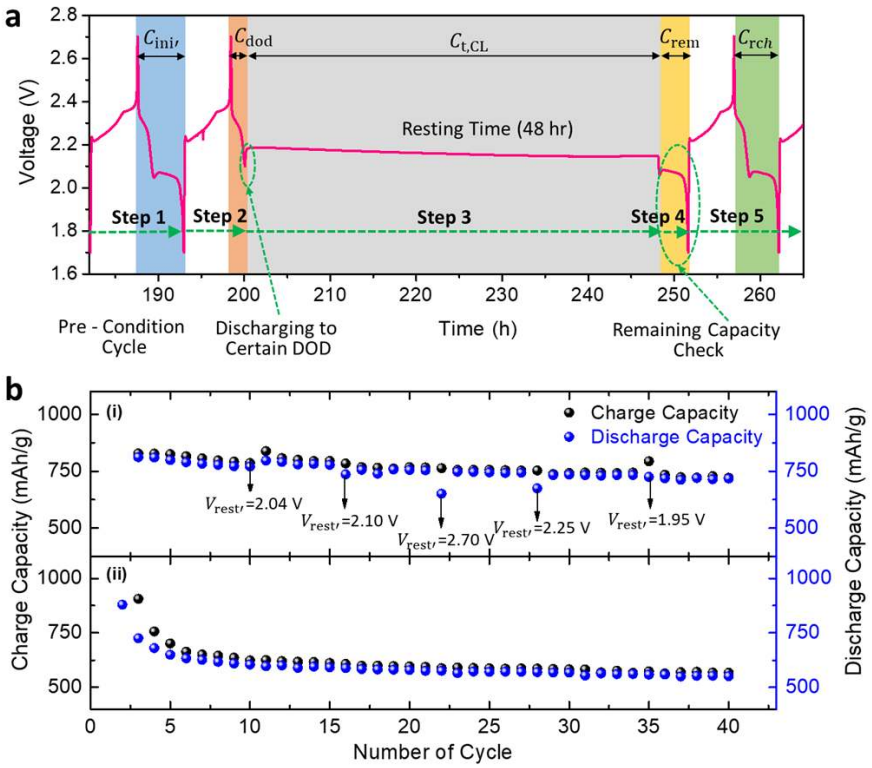

Figure 2. (a) Systematic protocol for self-discharge measurement (b) Variation of specific capacity as a function of cycle number (i) over different self-discharge periods of 48 hr at certain voltages (ii) without self-discharge periods.

Table 2. The DOD chosen for self-discharge measurements

Experiment		Simulation	
DOD′ (%)	$V_{rest'}$ (V)	DOD (%)	V_{rest} (V)
0	2.70	0	2.65
22	2.25	16	2.20
30	2.10	25	2.10
81	2.04	74	1.95
94	1.95	98	1.90

DOD′ and $V_{rest'}$ means the experimental results; DOD and V_{rest} come from simulation data.

In order to simulate the species distribution under the same resting states as the experiments, we chose the specific simulation voltages (V_{rest}) to keep the simulation DOD levels close to the experimental DOD′ levels. Due to differences in the voltage profiles between simulation and experiment, it was not possible to match DOD′ or $V_{rest'}$ in the simulation and thus intermediate values were chosen. The detailed experimental and simulation values are shown in Table 2.

The localized current density of five separate cathodic reactions are shown in Figure 1e. Reaction C1 occurs first and is followed by the conversion from longer PSs to shorter PSs. As shown in Figure 1d, there are four distinct sections on discharging voltage profile, labeled as S1-S4. In region S1, the discharge profile is dominated by Reaction C1, corresponding to the reduction of S_8. Region S2 involves Reaction C2 and C3 representing further reduction of S_8 to S_6^{2-} and S_4^{2-}. Region S1 and S2 are related to the dissolution of PSs and it delivers ¼ of the theoretical capacity (418 mA g^{-1}) due to ½ electron transfer per sulfur atom. Reaction C4 and C5 control discharging in S3 and S4 regions, and contribute to the precipitation reaction of solid phase reaction. The concentration variations further uncover

the evolution of different PSs. Figure 1f and 1g show the simulated concentration variations of PS during discharge-charge cycles under logarithmic scale and linear scales separately. The logarithmic scale more clearly displays the detailed concentration variations during the charge/discharge while the linear scale gives us an intuitive idea of the concentration distribution of ionic species. Figures S6 and S7 further confirmed the formation of PSs during one discharge-charge cycle and the spatial concentration distributions of Li_2S_2(s), Li_2S(s), and S_8(s) through the simulation domain.

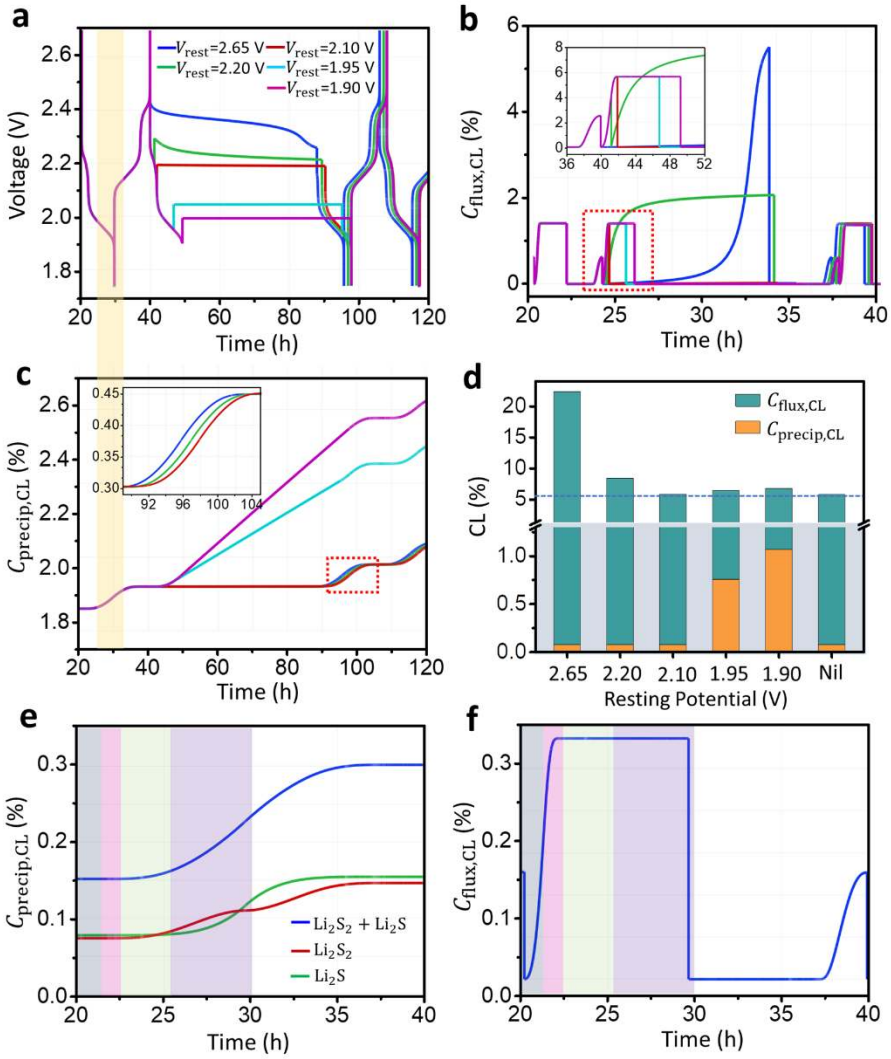

Figure 3. Simulated (a) voltage profiles, (b) self-discharge CL ($C_{flux,CL}$) profiles and (c) precipitation CL ($C_{precip,CL}$) profiles during cycling and resting. The legends in (b, c) are as the same as in (a). The yellow color bar highlights the discharge-charge cycle at the lower voltage plateau. (d) CL profiles during different resting potentials. Nil: CL during one discharge-charge cycle. (e) Precipitation CL profiles and (f) self-discharge CL profiles during one charge/discharge cycle. The color map in e, f is the same as Figure 1d-g.

3.2. Capacity loss. Figure 2a illustrates the procedure used to quantify CL as detailed above in Section 2.3. The plot of specific capacity as a function of cycle number exhibited by the a-graphene/S cathode at 0.1 C rested for 48 hr at different DOD′ level is shown in Figure 2b. It exhibits an initial discharge capacity of ~ 811 mAh/g. As typical for Li-S batteries, the capacity decays more rapidly over the initial cycles. But, the capacity decay stabilized afterwards and both the samples (Figure 2b (i) and (ii)) with and without self-discharge shows similar capacity decay of ≈ 0.002% at the end of cycling. However, the drop-in discharge capacity is different at different DOD′ level (as shown in Figure S8). When the cell was held for self-discharge during the 8th cycle (DOD′ ≈ 81% at 2.04 V), the capacity drops noticeably; however, this loss is recovered during the 9th cycle and $C_{t,CL} \approx C_{rev,CL}$. Similarly, resting the cell at ≈ 30 % and ≈ 0 % DOD′ causes an irreversible drop of the discharge capacity (values of capacity drop are given in Table S5). Resting at ≈ 22 % and ≈ 90 % DOD′ results in negligible loss of $C_{ir,CL}$. As shown in Figure S9, the sequence (and thus cycle-number) of these self-discharge measurements for one cell had little to no effect on the results. $C_{rev,CL}$ is close to zero after the higher voltage plateau because the diffusion and reaction

kinetics at the anode are very slow for the lower order PS (in the simulation). The $C_{ir,CL}$ is due to the precipitation, and this is shown to be irreversible by the monotonic increase in the precipitation of Li_2S_2 and Li_2S.

The full capacity of the Li-S battery was estimated by complete discharge of the battery immediately after fully charging at C/10. However, as self-discharge is taking place, the obtained capacity is less than total expected capacity.

Figure 3a depicts the simulated voltage profiles during rest and over the simulated charge and discharge carried out before and after the resting to mimic the experimental design. For example, as shown in Figure 3b, $C_{flux,CL}$, which accounts for these shuttling species, is 22.3 % when resting at 2.65 V. This shuttle phenomena leads to high rates of self-discharge, so the cell voltage decreases quickly during idling. However, the CL is reversible at these cell voltages, so this form of self-discharge does not cause irreparable battery degradation. On the other hand, resting the cell at lower voltages is problematic because the shorter-chain PS are the dominant species in the cell at these states of charge ($C_{precip,CL}$, Figure 3c), and these precipitate to form Li_2S_2 and Li_2S in the electrolyte and at the anode side. Ex-situ XRD (Figure S10) was carried out that provided some support for the formation of Li_2S on the Li anode. The potentially amorphous nature and low concentration make Li_2S_2 and Li_2S it difficult to observe experimentally. Figure 3d shows the predicted values of $C_{flux,CL}$ and $C_{precip,CL}$. When resting the Li-S battery at 2.1 V, both reversible and irreversible CL is minimized, thus this is the suggested resting potential for Li-S batteries.

The degradation model contains the accumulation of precipitates and evolution of self-discharge. The last column in Figure 3d is the variation of $C_{flux,CL}$ and $C_{precip,CL}$ during one continuous charge/discharge cycle without resting the cell, which are 5.71% and 0.075%, respectively. The CL resulting from self-discharge due to the shuttle flux ($C_{flux,CL}$) during one cycle is significantly larger than the irreversible precipitation CL ($C_{precip,CL}$). The detailed evolution of these two CL is depicted in Figure 3e and 3f. $C_{flux,CL}$ is fast at the higher voltage plateau while $C_{precip,CL}$ keeps increasing at the lower voltage plateau during a charge/discharge cycle.

Figure 4 is the comparison of experimentally observed CL due to self-discharge and the simulated behavior during resting. The experimental data is calculated using coulomb counting, while the modelled result used the intrinsic approach. Error bars for $C_{rev,CL}$represent the standard deviation in reversible capacity loss of four different self-discharge tests. An inverse relation between DOD and self-discharge can be observed (with increasing the DOD the self-discharge is decreasing). This qualitative trend has also been reported by the experimental work of Knap et al. who looked at the self-discharge of Li-S pouch cells.[26] $C_{flux,CL}$ is the total self-discharge CL and related to the shuttle flux and reduction reactivity of $S_8(l)$, S_8^{2-}, S_6^{2-}, S_4^{2-} S_2^{2-}, and S^{2-} species at the anode. The values of $C_{flux,CL}$ used in Figure 4 were reduced by 5%, meaning CL due to self-discharge during rest period. (the self-discharge flux during one discharge-charge cycle, is 5%, Nil case in Figure 3d). At the higher DOD, the shorter PSs, especially S_2^{2-} and S^{2-}, were the predominant species in the cell. The low-chain PSs leads to precipitation, which cannot be recovered during the following cycles.[52]

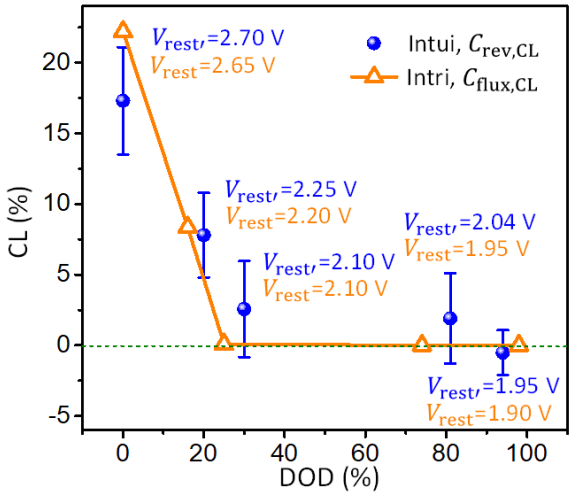

Figure 4. Comparison of CL between simulation and experimental data.

4. CONCLUSIONS

In this work a 1D Li-S battery model was presented to investigate reversible and irreversible capacity losses for long periods of cycling and especially during resting over a large voltage range. An extensive set of experiments and sensitivity analysis was conducted to validate the model parameters. The study provides insights into a key relationship among the rate of self-discharge, polysulfides shuttling, and the resting voltages. Based on simulation data, an intrinsic definition of self-discharge capacity loss is proposed, which is more accurate than the intuitive definition typically used based on Coulomb counting. It uncovers that resting the cell at the higher voltage plateau suffers rapid self-discharge losses due to fast reduction of longer-chain PS at the anode, while resting at the lower voltage plateau results in precipitation formation. Our model suggests Li-S batteries should be better held at around 2.10 V where S_4^{2-} is the predominate species. Noticeably, the model suggests that the focus to avoid self-discharge should be on suppressing the reduction of PSs on the anode instead of controlling the shuttling in the electrolyte during rest state. With a firmer grasp of the key parameters required to accurately model long-term cycling, the study provides a useful basis for further engineering of these parameters. The model can be applied to other phenomena in future studies and with other sizes and types of cells.

ASSOCIATED CONTENT

Supporting Information.

The Supporting Information is available free of charge via the Internet at http://pubs.acs.org.

Details model descriptions including the procedure of parameters fittings; Supporting tables of stoichiometries for each species, transport properties and reference concentrations, precipitation parameters, other constant parameters, and reversible and irreversible capacity losses calculated using the equations (11-14); Supporting figures of the

sensitivity analyses of the formal potential potentials, exchange current densities, reference concentration, precipitation reaction rates, and chemical overpotentials; Supporting figures of simulated concentration variations of PSs during one discharge-charge cycle, spatial concentration distributions of Li_2S_2(s) and Li_2S(s); experimental voltage profiles of the interrupted discharge plot at various resting voltages and the next immediate charge, variation of specific capacity as a function of cycle number over different self-discharge period for different cycles, and XRD patterns of various battery cell components.

AUTHOR INFORMATION

Corresponding Authors

* Jeff T. Gostick, Email: jgostick@uwaterloo.ca;
* Michael A. Pope, Email: michael.pope@uwaterloo.ca.

Author Contributions

G. W., S. R., and T. T. contributed equally to this work.

ACKNOWLEDGMENT

The authors gratefully acknowledge the support provided by the Natural Sciences and Engineering Research Council of Canada (NSERC), University of Waterloo, and Waterloo Institute for Nanotechnology. Specifically, S.R. and M.P. acknowledge NSERC's Collaborative Research & Development program and NanoXplore Inc. G. W. acknowledges the support from the China Scholarship Council (CSC). DB would like to acknowledge DST SERB for financial support, File no. ECR/2018/001039.

REFERENCES

(1) Pang, Q.; Kundu, D.; Cuisinier, M.; Nazar, L. F. Surface-Enhanced Redox Chemistry of Polysulphides on a Metallic and Polar Host for Lithium-Sulphur Batteries. *Nat. Commun.* **2014**, *5*, 1–8.

(2) Pope, M. A.; Aksay, I. A. Structural Design of Cathodes for Li-S Batteries. *Adv. Energy Mater.* **2015**, *5*, 1–22.

(3) Li, G.; Wang, X.; Seo, M. H.; Li, M.; Ma, L.; Yuan, Y.; Wu, T.; Yu, A.; Wang, S.; Lu, J.; et al. Chemisorption of Polysulfides through Redox Reactions with Organic Molecules for Lithium-Sulfur Batteries. *Nat. Commun.* **2018**, *9*, 1–10.

(4) Waluś, S.; Barchasz, C.; Colin, J.-F. F.; Martin, J.-F. F.; Elkaïm, E.; Leprêtre, J.-C. C.; Alloin, F. New Insight into the Working Mechanism of Lithium–Sulfur Batteries: In Situ and Operando X-Ray Diffraction Characterization. *Chem. Commun.* **2013**, *49*, 7899–7901.

(5) Li, G.; Wang, S.; Zhang, Y.; Li, M.; Chen, Z.; Lu, J. Revisiting the Role of Polysulfides in Lithium–Sulfur Batteries. *Adv. Mater.* **2018**, *30*, 1–19.

(6) Conder, J.; Bouchet, R.; Trabesinger, S.; Marino, C.; Gubler, L.; Villevieille, C. Direct Observation of Lithium Polysulfides in Lithium-Sulfur Batteries Using Operando X-Ray Diffraction. *Nat. Energy* **2017**, *2*, 17069.

(7) Kamphaus, E. P.; Balbuena, P. B. Effects of Dimethyl Disulfide Cosolvent on Li-S Battery Chemistry and Performance. *Chem. Mater.* **2019**, *31*, 2377–2389.

(8) Manthiram, A.; Fu, Y.; Chung, S. H.; Zu, C.; Su, Y. S. Rechargeable Lithium-Sulfur Batteries. *Chem. Rev.* **2014**, *114*, 11751–11787.

(9) Drvarič Talian, S.; Kapun, G.; Moškon, J.; Vizintin, A.; Randon-Vitanova, A.; Dominko, R.; Gaberščček, M. Which Process Limits the Operation of a Li-S System? *Chem. Mater.* **2019**, *31*, 9012–9023.

(10) Lin, Z.; Liu, Z.; Fu, W.; Dudney, N. J.; Liang, C. Phosphorous Pentasulfide as a Novel Additive for High-Performance Lithium-Sulfur Batteries. *Adv. Funct. Mater.* **2013**, *23*, 1064–1069.

(11) Wu, F.; Lee, J. T.; Nitta, N.; Kim, H.; Borodin, O.; Yushin, G. Lithium Iodide as a Promising Electrolyte Additive for Lithium-Sulfur Batteries: Mechanisms of Performance Enhancement. *Adv. Mater.* **2015**, *27*, 101–108.

(12) Salvatierra, R. V.; López-Silva, G. A.; Jalilov, A. S.; Yoon, J.; Wu, G.; Tsai, A. L.; Tour, J. M. Suppressing Li Metal Dendrites Through a Solid Li-Ion Backup Layer. *Adv. Mater.* **2018**, *30*, 1803869.

(13) Ghosh, D.; Gad, M.; Lau, I.; Pope, M. A. Trapping and Redistribution of Hydrophobic Sulfur Sols in Graphene-Polyethyleneimine Networks for Stable Li-S Cathodes. *Adv. Energy Mater.* **2018**, *8*, 1801979.

(14) Sun, Z.; Zhang, J.; Yin, L.; Hu, G.; Fang, R.; Cheng, H. M.; Li, F. Conductive Porous Vanadium Nitride/Graphene Composite as Chemical Anchor of Polysulfides for Lithium-Sulfur Batteries. *Nat. Commun.* **2017**, *8*, 14627.

(15) Li, Y.; Ye, D.; Liu, W.; Shi, B.; Guo, R.; Zhao, H.; Pei, H.; Xu, J.; Xie, J. A MnO2/Graphene Oxide/Multi-Walled Carbon Nanotubes-Sulfur Composite with Dual-Efficient Polysulfide Adsorption for Improving Lithium-Sulfur Batteries. *ACS Appl. Mater. Interfaces* **2016**, *4*, 28566–28573.

(16) Rehman, S.; Tang, T.; Ali, Z.; Huang, X.; Hou, Y. Integrated Design of MnO2 @Carbon Hollow Nanoboxes to Synergistically Encapsulate Polysulfides for Empowering Lithium Sulfur Batteries. *Small* **2017**, *13*, 1700087.

(17) Li, G.; Lei, W.; Luo, D.; Deng, Y.; Deng, Z.; Wang, D.; Yu, A.; Chen, Z. Stringed "Tube on Cube" Nanohybrids as Compact Cathode Matrix for High-Loading and Lean-Electrolyte Lithium-Sulfur Batteries. *Energy Environ. Sci.* **2018**, *11*, 2372–2381.

(18) Wang, X.; Li, G.; Li, J.; Zhang, Y.; Wook, A.; Yu, A.; Chen, Z. Structural and Chemical Synergistic Encapsulation of Polysulfides Enables Ultralong-Life Lithium-Sulfur Batteries. *Energy Environ. Sci.* **2016**, *9*, 2533–2538.

(19) Luo, D.; Li, G.; Deng, Y. P.; Zhang, Z.; Li, J.; Liang, R.; Li, M.; Jiang, Y.; Zhang, W.; Liu, Y.; et al. Synergistic Engineering of Defects and Architecture in Binary Metal Chalcogenide toward Fast and Reliable Lithium–Sulfur Batteries. *Adv. Energy Mater.* **2019**, *9*, 1–10.

(20) Ghazi, Z. A.; He, X.; Khattak, A. M.; Khan, N. A.; Liang, B.; Iqbal, A.; Wang, J.; Sin, H.; Li, L.; Tang, Z. MoS2 /Celgard Separator as Efficient Polysulfide Barrier for Long-Life Lithium-Sulfur Batteries. *Adv. Mater.* **2017**, *29*, 1606817.

(21) Rehman, S.; Guo, S.; Hou, Y. Rational Design of Si/SiO2@Hierarchical Porous Carbon Spheres as Efficient Polysulfide Reservoirs for High-Performance Li-S Battery. *Adv. Mater.* **2016**, *28*, 3167–3172.

(22) Liang, X.; Hart, C.; Pang, Q.; Garsuch, A.; Weiss, T.; Nazar, L. F. A Highly Efficient Polysulfide Mediator for Lithium-Sulfur Batteries. *Nat. Commun.* **2015**, *6*, 5682.

(23) Fan, L.; Li, M.; Li, X.; Xiao, W.; Chen, Z.; Lu, J. Interlayer Material Selection for Lithium-Sulfur Batteries. *Joule* **2019**, *3*, 361–386.

(24) Cañas, N. A.; Hirose, K.; Pascucci, B.; Wagner, N.; Friedrich, K. A.; Hiesgen, R. Investigations of Lithium-Sulfur Batteries Using Electrochemical Impedance Spectroscopy. *Electrochim. Acta* **2013**, *97*, 42–51.

(25) Mikhaylik, Y. V.; Akridge, J. R. Polysulfide Shuttle Study in the Li/S Battery System. *J. Electrochem. Soc.* **2004**, *151*, A1969–A1976.

(26) Knap, V.; Stroe, D.-I.; Swierczynski, M.; Teodorescu, R.; Schaltz, E. Investigation of the Self-Discharge Behavior of Lithium-Sulfur Batteries. *J. Electrochem. Soc.* **2016**, *6*, A911–A916.

(27) Chung, S. H.; Manthiram, A. Lithium-Sulfur Batteries with the Lowest Self- Discharge and the Longest Shelf Life. *ACS Energy Lett.* **2017**, *2*, 1056–1061.

(28) Ryu, H. S.; Ahn, H. J.; Kim, K. W.; Ahn, J. H.; Lee, J. Y.; Cairns, E. J. Self-Discharge of Lithium-Sulfur Cells Using Stainless-Steel Current-Collectors. *J. Power Sources* **2005**, *140*, 365–369.

(29) Ryu, H. S.; Ahn, H. J.; Kim, K. W.; Ahn, J. H.; Cho, K. K.; Nam, T. H. Self-Discharge Characteristics of Lithium/Sulfur Batteries

Using TEGDME Liquid Electrolyte. *Electrochim. Acta* **2006**, *52*, 1563–1566.

(30) Wild, M. Lithium Sulfur Batteries, a Mechanistic Review. *Energy Environ. Sci.* **2015**, *8*, 3477–3494.

(31) Knap, V.; Stroe, D.-I.; Swierczynski, M.; Purkayastha, R.; Propp, K.; Teodorescu, R.; Schaltz, E. A Self-Discharge Model of Lithium-Sulfur Batteries Based on Direct Shuttle Current Measurement. *J. Power Sources* **2016**, *336*, 325–331.

(32) Diao, Y.; Xie, K.; Xiong, S.; Hong, X. Shuttle Phenomenon – The Irreversible Oxidation Mechanism of Sulfur Active Material in Li–S Battery. *J. Power Sources* **2013**, *235*, 181–186.

(33) Cañas, N. A.; Wolf, S.; Wagner, N.; Friedrich, K. A. In-Situ X-Ray Diffraction Studies of Lithium–Sulfur Batteries. *J. Power Sources* **2013**, *226*, 313–319.

(34) Hofmann, A. F.; Fronczek, D. N.; Bessler, W. G. Mechanistic Modeling of Polysulfide Shuttle and Capacity Loss in Lithium-Sulfur Batteries. *J. Power Sources* **2014**, *259*, 300–310.

(35) Busche, M. R.; Adelhelm, P.; Sommer, H.; Schneider, H.; Leitner, K.; Janek, J. Systematical Electrochemical Study on the Parasitic Shuttle-Effect in Lithium-Sulfur-Cells at Different Temperatures and Different Rates. *J. Power Sources* **2014**, *259*, 289–299.

(36) Marinescu, M.; Zhang, T.; Offer, G. J. A Zero Dimensional Model of Lithium-Sulfur Batteries during Charge and Discharge. *Phys. Chem. Chem. Phys.* **2016**, *18*, 584–593.

(37) Kumaresan, K.; Mikhaylik, Y.; White, R. E. A Mathematical Model for a Lithium–Sulfur Cell. *J. Electrochem. Soc.* **2008**, *155*, A576–A582.

(38) Wild, M.; O'Neill, L.; Zhang, T.; Purkayastha, R.; Minton, G.; Marinescu, M.; Offer, G. J. Lithium Sulfur Batteries, a Mechanistic Review. *Energy Environ. Sci.* **2015**, *8*, 3477–3494.

(39) Vélez, P.; Para, M. L.; Luque, G. L.; Barraco, D.; Leiva, E. P. M. Modeling of Substitutionally Modified Graphene Structures to Prevent the Shuttle Mechanism in Lithium-Sulfur Batteries. *Electrochim. Acta* **2019**, *309*, 402–414.

(40) Jia, J.; Wang, K.; Zhang, X.; Sun, X.; Zhao, H.; Ma, Y. Graphene-Based Hierarchically Micro/Mesoporous Nanocomposites as Sulfur Immobilizers for High-Performance Lithium-Sulfur Batteries. *Chem. Mater.* **2016**, *28*, 7864–7871.

(41) Ghaznavi, M.; Chen, P. Analysis of a Mathematical Model of Lithium-Sulfur Cells Part III: Electrochemical Reaction Kinetics, Transport Properties and Charging. *Electrochim. Acta* **2014**, *137*, 575–585.

(42) Ghaznavi, M.; Chen, P. Sensitivity Analysis of a Mathematical Model of Lithium-Sulfur Cells: Part II: Precipitation Reaction Kinetics and Sulfur Content. *J. Power Sources* **2014**, *257*, 402–411.

(43) Albertus, P.; Christensen, J.; Newman, J. Modeling Side Reactions and Nonisothermal Effects in Nickel Metal-Hydride Batteries. *J. Electrochem. Soc.* **2008**, *155*, A48–A60.

(44) Kumaresan, K.; Mikhaylik, Y.; White, R. E. A Mathematical Model for a Lithium-Sulfur Cell. *J. Electrochem. Soc.* **2008**, *155*, A576–A582.

(45) Cheon, S.-E.; Ko, K.-S.; Cho, J.-H.; Kim, S.-W.; Chin, E.-Y.; Kim, H.-T. Rechargeable Lithium Sulfur Battery. *J. Electrochem. Soc.* **2003**, *150*, A796.

(46) Shen, C.; Andrei, P.; Zheng, J. P. Unraveling the Li2S Deposition Process on a Polished Graphite Cathode for Enhancing Discharge Capacity of Lithium–Sulfur Batteries. *ACS Appl. Energy Mater.* **2019**, *2*, 3860–3868.

(47) Shen, C.; Andrei, P.; Zheng, J. P. Stable Cycling of Lithium-Sulfur Batteries by Optimizing the Cycle Condition. *Electrochim. Acta* **2019**, *326*, 134948.

(48) Yi, Z.; Su, F.; Huo, L.; Cui, G.; Zhang, C.; Han, P.; Dong, N.; Chen, C. New Insights into Li2S2/Li2S Adsorption on the Graphene Bearing Single Vacancy: A DFT Study. *Appl. Surf. Sci.* **2020**, *503*, 144446.

(49) Bard, A. J.; Faulkner, L. R. *Electrochemical Methods: Fundamentals and Applications,* 2nd ed.; John Wiley & Sons, inc.: New York, 2001.

(50) Mistry, A. N.; Mukherjee, P. P. "Shuttle" in Polysulfide Shuttle: Friend or Foe? *J. Phys. Chem. C* **2018**, *122*, 23845–23851.

(51) Knap, V.; Stroe, D.-I.; Swierczynski, M.; Teodorescu, R.; Schaltz, E. Investigation of the Self-Discharge Behavior of Lithium-Sulfur Batteries. *J. Electrochem. Soc.* **2016**, *163*, A911–A916.

(52) Shen, C.; Xie, J.; Zhang, M.; Andrei, P.; Hendrickson, M.; Plichta, E. J.; Zheng, J. P. Self-Discharge Behavior of Lithium-Sulfur Batteries at Different Electrolyte/Sulfur Ratios. *J. Electrochem. Soc.* **2019**, *166*, A5287–A5294.

Table of Content (TOC):